

Pulse shaping effects on nanoparticle generation

Sid Senadheera

Ryerson University, 350 Victoria Street, Toronto, ON M5B 2K3, Canada

email : sid.senadheera@ryerson.ca
Phone : +1-647-202-8410

Abstract

Current research has not fully realized the advantages of pulse shaping in areas such as nanoparticle generation by femtosecond laser ablation. In this paper, we have summarized our findings on how the nanoparticle aggregate generation process is affected by the use of a double pulse ablation and how this process is further manipulated to increase yield by using certain amounts of energy in each pulse. It was found that by using a given ratio of energy for the two pulses can result in a higher amount of nanoparticle generation. Previous scientific research in this area experimentally proved that the ratio of the produced Si⁺/Si (or Si-II/Si-I) decreases with time. We proved how this ratio decreases with time both theoretically and experimentally. This proof was speculated before by other researchers without enough theoretical explanation.

Keywords : double-pulse, ablation, femtosecond, Silicon, laser

1. Introduction

Femtosecond laser ablation is the explosive removal of material excited to extreme temperatures and pressures by absorbing high intensity laser pulses of sub-picosecond duration. The femtosecond laser ablation of Silicon in air ambient has been investigated extensively by many research groups []. Hydrodynamic theoretical models suggest that the nanoparticles form by a

mechanical fragmentation of a highly pressurized fluid undergoing rapid quenching during expansion in the vacuum [].

The ablated material acts as a superheated fluid as the laser energy increases. As the laser energy is further increased, the system relaxation path falls well above the critical point, thus leading to ablation outside the vapor-liquid metastable region. Nucleation cannot be accounted for as the main ablation mechanism in this process and given the large number of clusters present in the plume, vaporization must also be excluded. Therefore femtosecond laser ablation is not caused by a photothermal process but may have, in this case, a mechanical origin as well. Fragmentation results from the conversion of the internal stress stored in the expanding target into surface energy: when the elastic energy stored in a region of the target is equal to the surface energy, the excess elastic energy is converted into surface energy and fragments are created. Experimental studies of evolution of the ablation of silicon supported this theoretical prediction and showed that the ablated material is composed almost entirely of ejected liquid silicon with very little vapor []. In addition, it was found that the nanoparticles form within 50ps by a non-equilibrium, nonthermal phase transformation rather than by a thermal nucleation and growth process [].

3.Experimental setup for double pulse femtosecond laser ablation

Researchers have developed many methods for generating nanoparticles and nanomaterials. Pulsed Laser Ablation (PLA), whereby a material is evaporated by an intense laser pulse in the femtosecond regime, is the preferred method that we used. It is a well-known technique for thin film deposition as well as for the preparation of nanoparticles and nanomaterials [].

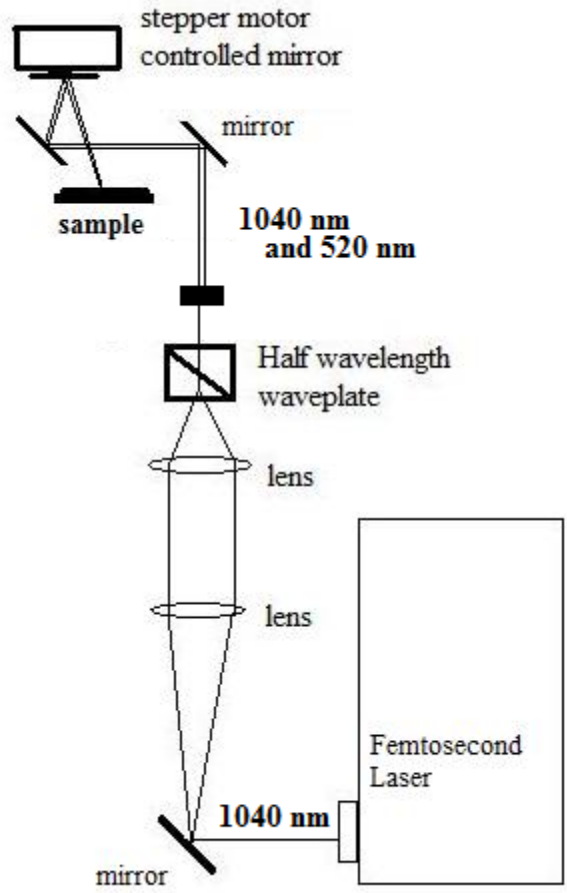


Figure [] : Double pulse generating system

We used a femtosecond laser capable of producing variable pulse widths and pulse frequencies. The laser source is an all-diode-pumped, direct-diode pumped Yb-doped fiber oscillator-amplifier system capable of producing variable pulse energies up to 10 mJ at a pulse frequency between 200 kHz and 25 MHz. Average power varies between 0-20W. Arrays of microvias were drilled into a Silicon target with laser beam at various pulse frequencies and varying energies between the two pulses. The samples were then characterized using scanning electrical microscopy (SEM).

2.THEORETICAL MODEL

A detailed understanding of mutual interactions among the heat carriers, e.g., photons, electrons (holes), and phonons, is required for analyzing microscale heat transfer phenomena. For situations in which the carrier temperature is much higher than the lattice temperature owing to ultrashort pulse laser heating, especially, a consistent theoretical model should be derived that is able to mimic the nonequilibrium between carriers and lattice. In the case that photons incident on semiconductor have energies greater than the band gap energy of the material, the main heat carrier is an electron–hole pair, whereas it is the free electron for metals [11, 15, 17]. The carrier number density of electron–hole pairs, N_C , is determined from the following conservation equation:

$$\frac{\partial N_C}{\partial t} = \frac{\alpha_1 I}{h\nu} - \gamma N_C^3$$

where t is time, g is the Auger recombination rate, N_C is the carrier number density, h is the Planck constant, I is the laser intensity as a function of time and space, ν is the photon frequency, and α_1 is one photon band-to-band absorption coefficient. The temporal change of the carrier number density is governed by two terms on the right-hand side of Equation []. One of these is the absorption source term that corresponds to direct transition that excites an electron to the conduction band and creates an electron–hole pair, and the other gives the loss of the carriers through Auger recombination process in which the free electrons are captured by ionized donors and lose their energy nonradiatively []. Because the size of the laser beam is large compared to the laser penetration depth, short-pulse laser heating of materials can be modeled as one-

dimensional. A set of consistent models for the nonequilibrium thermal system is composed of two standard parts, one of which is the carrier transport equation and the other the lattice one, as follows []:

$$\frac{\partial U_C}{\partial t} = \frac{\partial}{\partial y} \left(\kappa_C \frac{\partial T_C}{\partial y} \right) - \frac{3N_C k_B}{\tau_C} (T_C - T_L) + \alpha I$$

$$\frac{\partial U_L}{\partial t} = \frac{\partial}{\partial y} \left(\kappa_L \frac{\partial T_L}{\partial y} \right) + \frac{3N_C k_B}{\tau_C} (T_C - T_L)$$

Where U is the internal energy, y is the spatial coordinate, k is the thermal conductivity, k_B is the Boltzmann constant, τ_C is the carrier-to-phonon energy relaxation time, T is the temperature, and α is the absorption coefficient. On the right-hand side of Equation [], the first term is the heat diffusion due to carriers, the second represents the energy transfer from carriers to phonons during τ_C , and the third term is a source term due to photon absorption. Note that the assumption of Fourier law is not really valid for short-time-scale studies, but this is an approximation that invokes closure in the present type of hydrodynamic equation. In the present study, the non-equilibrium between the optical and acoustic phonons is not considered because the lattice is assumed to be a single thermodynamic system []. This implicitly assumes equilibrium between optical and acoustic phonons. Under the above assumptions, the internal energies of carrier and lattice, and the laser fluence, are described, respectively, as :

$$I = \frac{0.939J(1 - R)}{t_P} \exp\left(-\int_0^y \alpha dz\right) \exp\left(-\frac{2.773t^2}{t_P^2}\right)$$

Property	Value	Ref.
Heat capacity of the carriers (J/m ³ K)	$C_c = 3N_c k_B$	[19]
Heat capacity of the lattice (J/m ³ K)	$C_l = 2.07 \times 10^6$	[19]
Thermal conductivity of the carriers (W/m K)	$\kappa_c = -0.556 + 7.13 \times 10^{-3} T_c$	[19]
Thermal conductivity of the lattice (W/m K)	$\kappa_l = 1.585 \times 10^5 T_l^{-1.23}$	[15]
Energy relaxation time (s)	$\tau_c = \tau_\theta [1 + (N_c/N_{c,cr})^2]$ $\tau_\theta = 0.5 \times 10^{-12}$ $N_{c,cr} = 2 \times 10^{27}$	[15, 19]
Absorption coefficient (1/m)	$\alpha = \alpha_l + \sigma_{fc} N_c$ $\sigma_{fc} = 5.1 \times 10^{-23} [1.17/(h\nu)]^2 [T_l/300.]$	[21]
Auger recombination coefficient (m ⁶ /s)	$\gamma = 3.8 \times 10^{-43}$	[15]
Reflectivity	$R = 0.32$	[19]
Band gap (eV)	$E_g = 1.167 - 0.0258 [T_l/300.] - 0.0198 [T_l/300.]^2$	[21]

Some researchers [] indicated that the presence of the background gas (air in our case), irradiation fundamentally changes the mechanism for nanoparticle formation. Two phases have been observed in the collected plume material: spherical particles of crystalline silicon ranging in diameter from 50nm to 450 nm and a highly porous network of amorphous silicon with feature sizes ranging from 1 to 10 nm. They found that the crystalline nanoparticles are formed by thermal nucleation and growth; the crystalline phase forms from small droplets of liquid that are subjected to a high cooling rate []. As illustrated in Figure [], the following four regimes occur in succession before the creation of clusters and nanoparticle aggregates

- (1) Optical excitation of the target by the high energy laser photons by the femtosecond laser.
- (2) Lattice modifications and vibrations causing superheated emission of plasma [] and vapor.
- (3) Supercooling that starts the nucleation process during gas to liquid phase transition.
- (4) Material removal, ejection and creation of nanoparticles and nanoparticle aggregates.

Include a Figure [] to further elaborate (similar to Tinten and Sokolowski)

At the later stages of the formation of two fronts nanoparticle and atomic constituents of the plume is depicted by a schematic drawing in Figure []. To understand the formation of fractal nanoparticle aggregates, it is important to understand how the plume evolves with time after the laser ablation from the target. Characterizing experimental results with an SEM [], we observed that individual nanoparticles are bonded with each other to form nanoparticle aggregates, as shown in Figure[].

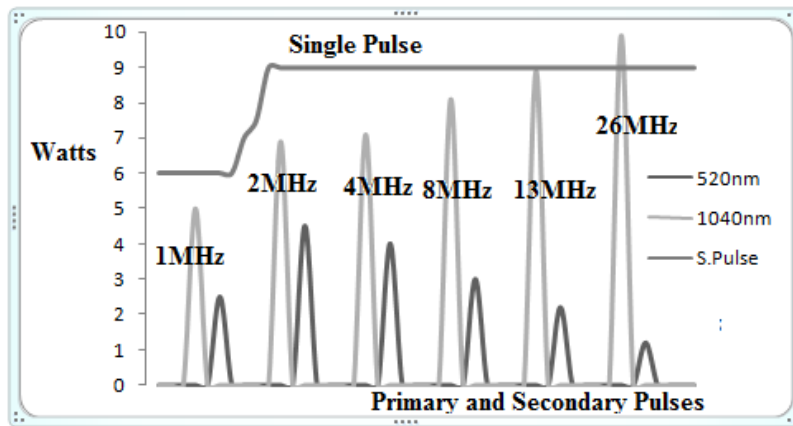


Figure []: At six different repetition rates, the double pulse profiles can be shown as above. The experiment was repeated for the single-pulse ablation for comparing results.

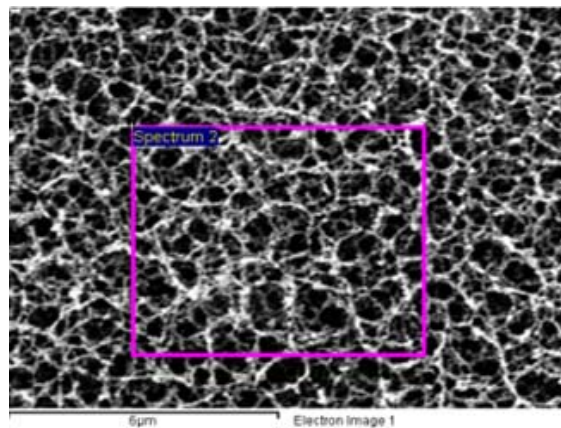


Figure []: The rectangular area marks where the spectral data was extracted

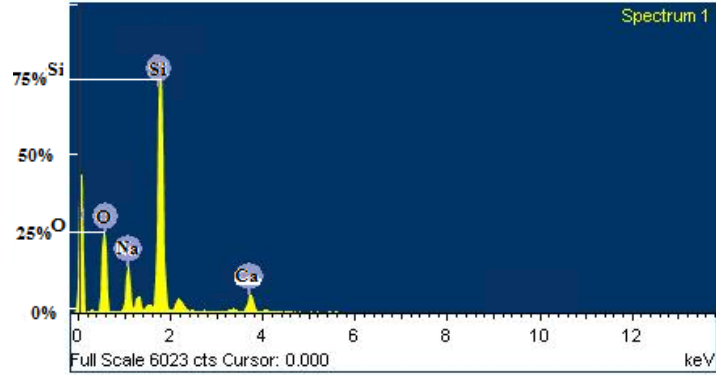


Figure [] : The above spectra obtained for the $6 \times 4 \mu\text{m}^2$ shows that the second most prominent line is Oxygen which are bonded to Si^+ ablated ions.

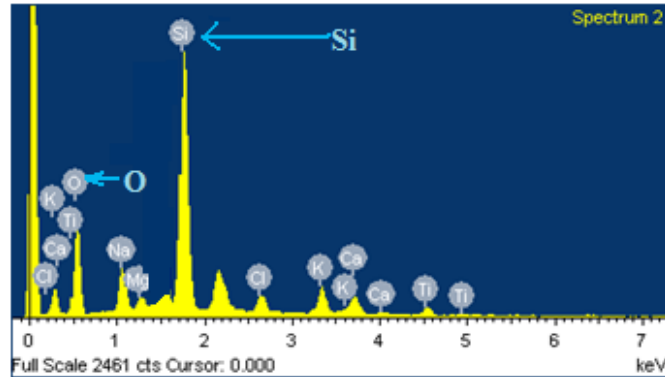


Figure [] : The above spectra obtained for a similar Silicon nanoparticle target shows that the Oxygen content is 1/3 rd of Silicon. Therefore Si^+ is 25% of the total ablation volume.

1MHz	2MHz	4MHz	8MHz	13MHz	25MHz
w1/w2	w1/w2	w1/w2	w1/w2	w1/w2	w1/w2
2	1.53	1.775	2.7	4.045	8.25

	MHz	E2	E1	E1/E2
(a)	1	2.5	5	2
	2	4.5	6.9	1.5333
	4	4	7.1	1.775
	8	3	8.1	2.7
	13	2.2	8.9	4.0455
(b)	26	1.2	9.9	8.25

1MHz	2MHz	4MHz	8MHz	13MHz	25MHz
7	9	9	9	9	9

Figure [] : The ratios of the double pulse laser (a) and the single pulse laser (b).

3. Results and discussion

Analyzing the spectrum **Figure []**, it was found that the nanoparticle aggregate material consisted mostly of Si and SiO (Si+) elements. This agrees with the findings of such researchers as : Narayanan et al. Appl. Surf. Science 222/382 (2004).

In this paper, we have shown that by choosing a certain ratio for Si+/Si elements femtosecond laser effects for Si nanoparticle generation could be maximized. We also proved that this ratio reduces with time, which has also been proved by other researchers using optical emission spectroscopy and T-O-F measurements of the ablation products.

As previously mentioned we found out that during the nanoparticle condensation phase, nanoparticles can condense in different forms. If the pulse frequency is high enough they would condense as 3D-fractal nanoparticle aggregates and keep building layers upward as each consecutive laser pulses occur. For lower pulse frequencies the nanoparticles would condense as spherical particles in Figure []. Therefore pulse frequency has a significant effect in creating fractal nanoparticle aggregates and keeping them continually forming. For high pulse frequencies, ablation from consecutive pulses happen before the material on the surface of the target cools down[]. Therefore the material that is ejected by a new pulse can have its ablated material condense (or bond) with the ablated material from the previous pulse which is still at a very high temperature. This is a possible explanation for how the nanoparticle structures are built dense three dimensionally.

Several studies on the mechanisms of laser absorption and material excitation, as well as its removal and expansion, have been done []. The detailed course of the very complex phenomenon occurring during the interaction depends strongly on the parameters of the laser pulse and the target material. Although femtosecond laser ablation differs from picosecond and

nanosecond laser ablation, the fundamental processes that occur can be described as following. However, even in the femtosecond case it will be explained how double pulse laser ablation would differ from the single pulse laser ablation.

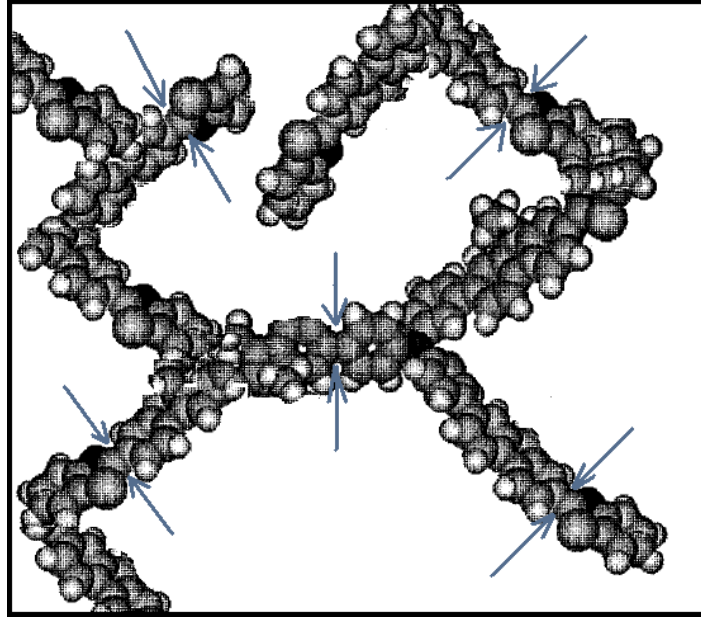


Figure [] : A strain of nanoparticles. By averaging the values with least thickness (given by the arrows) the mean value of the particle distribution can be calculated.

During the laser ablation the material inside the plume evolves through several physical states before condensation. In the first step the laser light is absorbed by free electrons due to inverse Bremsstrahlung process in the semiconductor at the top layer. This is followed by a fast energy transfer to the lattice owing to electron-phonon coupling. After the energy transfer, a high temperature is reached in the lattice. The interaction of intense ultrashort light pulses with the target leads to a phase transformation (melting of surface, evaporation and plasma formation). At first the very high heating rates cause a rapid melting and the transition to an overcritical fluid. An overcritical fluid occurs when the material is in a non-equilibrium state of high pressure and high temperature. The rapidly increasing vapor pressure near the surface

creates a large driving force for vapor expansion. The high temperature and the density lead to pressures far exceeding the background gas pressure (of the order of 10–100 atm). The unusually high fluid pressure causes the plume front to expand very rapidly with time in a highly forward-directed pattern. At early times, the plume front is spherical in nature, but as time evolves the plume front becomes sharpened Figure []. Along with sharpening, the expanding plume front splits into a fast and slow moving cloud indicating plume splitting [].

3.7. Laser energy levels and the ablation mechanism

To assure the validity of LTE approximation, collisions must dominate the energy-transfer processes and establish a Boltzmann distribution among the bound energy levels, the electron density, n_e must satisfy the following condition []:

$$n_e \geq 1.6 \times 10^{12} [T_e \text{ (K)}]^{1/2} [\Delta E]^3$$

The term ΔE is the energy difference between the upper and lower states, T_e (K) the electron temperature, n_e the lower limit for the electron number density. The estimated value of the lower limit of $n_e = 4.8 \times 10^{16} \text{ cm}^{-3}$ is obtained by using $\Delta E = 3 \text{ eV}$ for the transition at 413.09 nm while the Stark-broadened profile gives a value of $n_e = 1.2 \times 10^{18} \text{ cm}^{-3}$, two orders of magnitude higher than the lower limit justifies our use of LTE.

Since photon energy, $h\nu = 3.5 \text{ eV}$ of the ablating radiation is much less than the first ionization potential of Si (8.151 eV), the photoionization via three steps might be a dominant ionization mechanism. Once the plasma is initiated in the hot vapor, the absorption of laser radiation generally occurs via electron–neutral inverse bremsstrahlung and photoionization of the

TABLE II. Threshold fluences (F_{thres} , in J cm^{-2}) for observation of X^{z+} emissions under the prevailing experimental conditions together with threshold ionization energies (IE , in eV) for forming the various X^{z+} ions from the ground state neutral atom.

	C	Si	Cu	Al
$F_{\text{thres}}/\text{J cm}^{-2}$	12	5	4	<2
$IE (X \rightarrow X^+)/\text{eV}$	11.26	8.15	7.73	5.99
$IE (X \rightarrow X^{2+})/\text{eV}$	35.64	24.50	28.02	24.81
$IE (X \rightarrow X^{3+})/\text{eV}$	83.53	57.99	64.86	53.26
$IE (X \rightarrow X^{4+})/\text{eV}$	148.02	103.13	122.23	173.25

By Claeysens, Henley, and Ashfold, J. Appl. Phys., Vol. 94, No. 4, 15 August 2003 []

excited state atoms, for the UV radiation. However, when the sufficient ionization stage is reached (>1%), the dominant laser absorption mechanism makes a transition to electron-ion inverse bremsstrahlung []. It involves the absorption of a photon by a free electron during electron-ion collisions. The absorption coefficient is given by []:

$$\alpha(\text{cm}^{-1}) = (3.69 \times 10^8)(Z^3 n_e^2 / \sqrt{T} \nu^3) \{1 - e^{-\frac{h\nu}{kT}}\}$$

where Z , n_e and T are the atomic number, electron density in cm^{-3} , and electron temperature, respectively. Since $h\nu > kT$, the term $\{1 - e^{-\frac{h\nu}{kT}}\}$ can be approximated to unity. The absorption coefficient of $\alpha_p = 8.8 \times 10^{-2} \text{ cm}^{-1}$ is obtained for the electron-ion inverse bremsstrahlung. Absorption via photoionization can be estimated from [25]:

$$\alpha_{\text{pi}}(\text{cm}^{-1}) = \sum_n 7.9 \times 10^{18} \left(\frac{E_n}{h\nu}\right)^3 \left(\frac{I}{E_n}\right)^{1/2} N_n$$

where E_n and N_n are ionization energy and number density of the excited state 'n', respectively, and h is the Planck constant, ν the laser frequency and I the ionization potential of the ground

state atom. The absorption coefficient of the photoionization is obtained by summing up all, the excited states whose ionization energy is smaller than laser photon energy. The excitation potentials of atomic transitions of silicon atoms involved in the temperature calculations are higher than the laser photon energy (3.5 eV) used in this experiment, therefore the direct photoionization will not contribute to the absorption. Hence the possible mechanism for photoionization is simultaneous absorption of more than one photon.

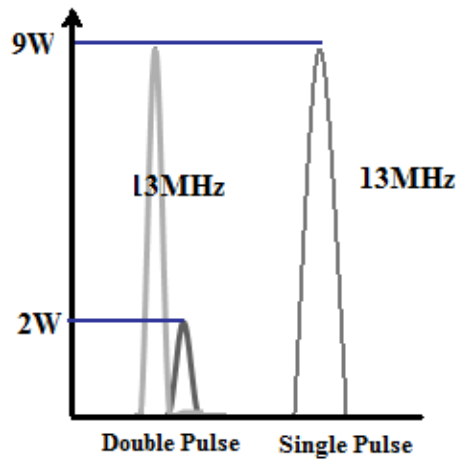
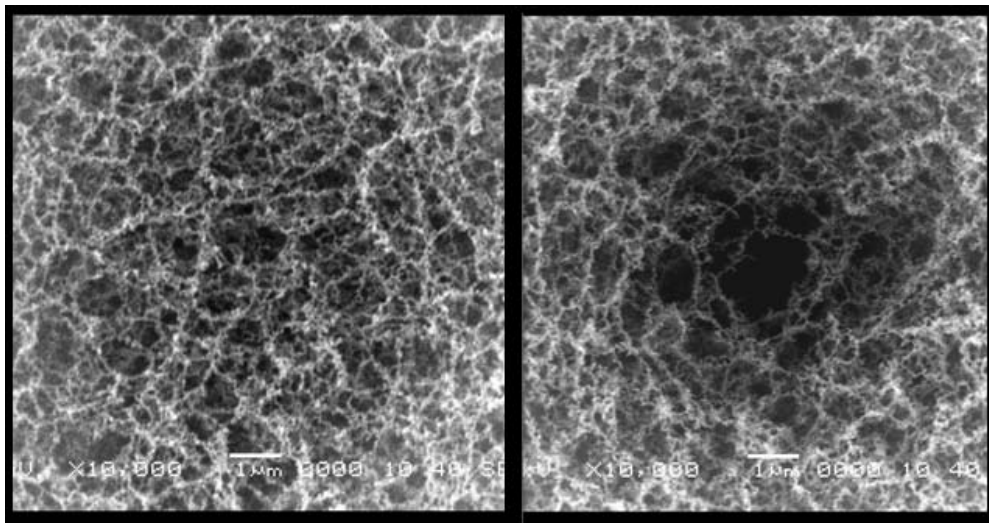


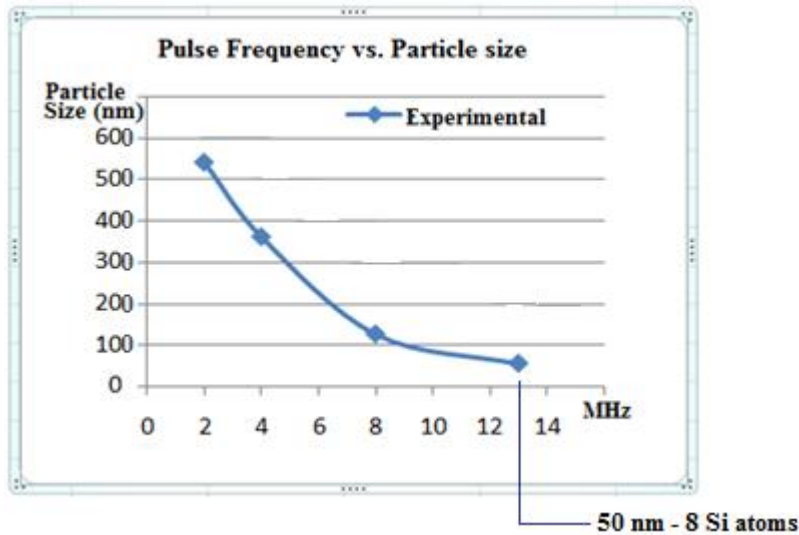
Figure [] : At 13 MHz with double pulse on left and single pulse on right. It can be seen clearly that the double pulse produced a higher concentration than the single pulse.

Crystal nucleation has been studied extensively by many researchers, yet the rate of crystal nucleation[11] and the distribution of sizes are exceedingly difficult to predict. According to semi-classical nucleation theory, the total free energy cost to form a spherical radial distribution of nanoparticles is given by [Ref 8, Anisimov et al]. The initial radii r_{pj} of the nanoparticles after condensation following the vacuum expansion is given by the equation [a] derived using [Ref. 2, R.Hergenroeder].

(Density) x (Volume of a cluster) = (Number of clusters) x (Mass of a single cluster)

$$\rho_L \left(\frac{4\pi}{3} \right) r_{pj}^3 = j \frac{g(t)M}{N_A} \quad - \text{Eqn: (a)}$$

$$r_{pj} = \left\{ \frac{3 g(t)}{4\pi} \cdot \left(\frac{j}{\rho_L} \right) \cdot M/N_A \right\}^{1/3}$$



Here $g(t)$ is the number of particles in a cluster given as a function of time. The numerical values for $g(t)$ has been used from 8 to 180 [Anisimov et al]. Using equation [a] the individual thicknesses of nanoparticles can be calculated and compared with experimental results as in

Figure []. Equation[a] gives average fragment sizes of ≈ 50 nm for the typical lattice temperature attained during femtosecond laser irradiation. We were able to prove that the theoretical sizes predicted by equation [a], closely agree with the measured experimental values Figure [].

The methodology in Figure [] was used to measure the widths of the nanoparticle aggregate chains. We observed the fractal nanoparticle aggregates from 2MHz until 13 MHz. Nanoparticles are bonded together to build nanoparticle aggregates (as beads). To measure the thickness of the nanoparticle aggregates, the thickness of several locations are measured and then averaged. In our estimates of the average thickness, we saw that the thickness decreased with increasing pulse frequency.

5. Proof of decreasing ratio of Si-II/Si-I with time

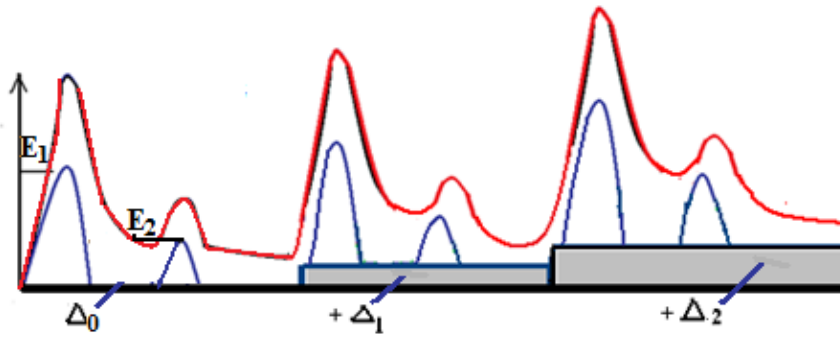


Figure [] : Consecutive pulses E1 and E2. The following two pulses accumulate the energy of from the two previous pulses. This process continues and reaches a plateau.

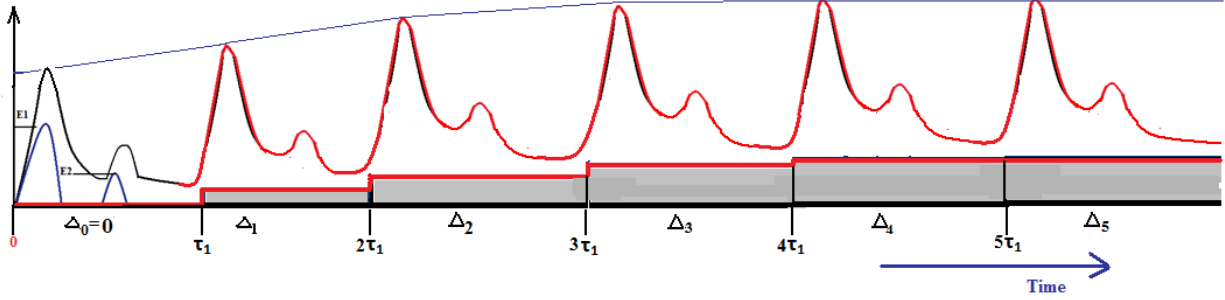
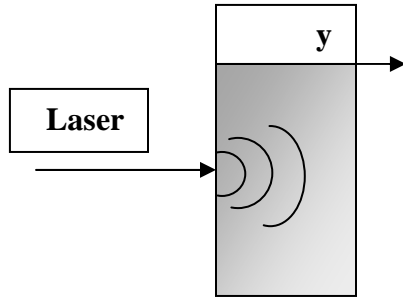


Figure []. τ_n is the 1/(repetition rate of the laser) measured in seconds. N is not only a function of E_1, E_2 - it is also a variable of increasing energy ΔE_n or $\Delta_n = \Delta_n (\Delta E_n)$

$$\frac{E_1 \text{ (pulse energy)}}{E_2 \text{ (pulse energy)}} = N$$



$$I = \frac{0.939J(1-R)}{t_p} \exp\left(-\int_0^y \alpha dz\right) \exp\left(-\frac{2.773t^2}{t_p^2}\right)$$

$$I = 0.939J(1-R)/t_p * \exp\left(-\int_0^y \alpha \cdot dy\right) \cdot \exp\left(-2.773 \frac{t^2}{t_p^2}\right)$$

$$\alpha(cm^{-1}) = (3.69 \times 10^8)(z^3 n_e^2 / \sqrt{T} v^3) \{1 - e^{-\frac{hv}{kT}}\}$$

After a time t_0 , the target absorbs $I(t_0)$ amount of energy.

$$I(t_0) = \frac{3.46 \times 10^8 J(1-R)}{t_p} \int_0^y (z^3 n_e^2 / \sqrt{T} v^3) \{1 - e^{-\frac{hv}{kT}}\} dy \cdot \exp\left(-2.773 \frac{t^2}{t_p^2}\right)$$

$$\text{Since } \frac{hv}{kT} \gg 1 : \left\{1 - e^{-\frac{hv}{kT}}\right\} \Rightarrow 1$$

$$I(t_0) = \frac{(3.69 \cdot 10^8) J(1-R)}{t_p} \int_0^y \left(\frac{z^3 n_e^2}{\sqrt{T} v^3} \right) dy \cdot \exp\left(-\frac{2.773 t^2}{t_p^2}\right)$$

$$I(t_0) \propto \left\{ \int_0^y \left(\frac{z^3 n_e^2}{\sqrt{T} v^3} \right) dy \right\} \cdot \exp\left(-\frac{2.773 t^2}{t_p^2}\right)$$

The function on the left, inside the integral path $0 \Rightarrow y$ increases and dominates in the beginning. The function with the exponential goes to zero as time goes to infinity. The product of the two would produce an initially increasing and then decreasing $I(t_0)$ just as what we expect from a femtosecond pulse laser. In a realistic model the inverse Brehmstrahlung function for energy absorption can be modeled in the above equation- []. A simpler function : $\Delta_n(t) = (1 - e^{-t})$ can be used to study the general behavior of the above complex function.

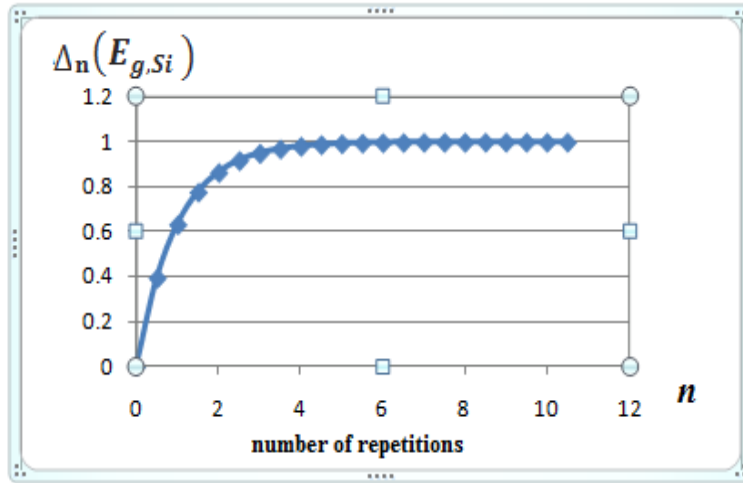


Figure [] : $\Delta_n(t) = (1 - e^{-t})$ graphed

$$N(1) = \frac{E_1 + \Delta_1(\Delta E_1)}{E_2 + \Delta_1(\Delta E_1)} \rightarrow N(2) = \frac{E_1 + \Delta_2(\Delta E_2)}{E_2 + \Delta_2(\Delta E_2)} \rightarrow N(3) = \frac{E_1 + \Delta_3(\Delta E_3)}{E_2 + \Delta_3(\Delta E_3)}$$

.....

Can be generalized as : $N(t) = \frac{E_1 + \Delta_n(\Delta E_n(t))}{E_2 + \Delta_n(\Delta E_n(t))}$ where $N(t) = Si_+(t)/Si(t)$

To simplify the analytical approach assume $\Delta E_n(t)$ varies with time in the following way,

$$N(n) = \frac{E_1 + (1 - e^{-t})}{E_2 + (1 - e^{-t})}$$

By numerically examining the general time dependence behavior of the Si+/Si ratio due to repetition rate for repetition rates $\tau_n = 2\text{MHz}, 4\text{MHz}, 8\text{MHz}, 13\text{MHz}, 26\text{MHz}$. The graphs in **Figure []** show the general behavior of how Si-II/S-I ratio is affected by the Inverse

Brehmstrahlung absorption. The ratio Si-II/Si-I decreases with time for higher repetition rates. The production of Si+ ceases after some time and all the absorbed energy goes into the production of Si. Our theoretical findings are in agreement with the experimental work that other researchers have conducted.

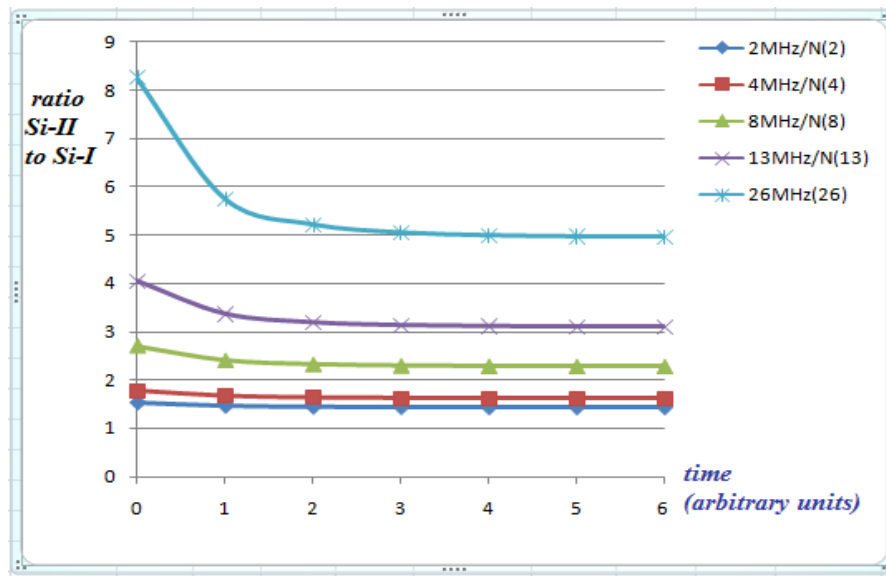


Figure [] : decreasing ratios of Si-II/Si-I with time due to changes in energy decay from consecutive pulses through Brehmstrahlung absorption

Ablated silicon by other researchers showed the presence of mostly Si-I and Si-II [3]. The relative concentration of Si-II/Si-I decrease away from the target surface. The optimization of

neutral concentration found at large distances from the target may be helpful in the formation of nanocrystalline silicon as in our case. The ambient environment being atmospheric air an absorption layer of high electron–ion density [32] may be formed above the target surface resulting in a high plasma pressure during the laser pulse. This may very well apply to our experimental setup as well. The high plasma pressure results in lateral plasma compression wave leading to change in energy distribution on the target.

Si-I forms after 50 ns and lasting till 450 ns whereas Si-II has maximum intensity at 50 ns and disappears after 150 ns implying that Si-I originates from recombination of Si-II. This suggest that the nucleation of clusters start with Si I, which, after condensation, gets deposited onto the suitably placed substrate. Ratio of Si-II/Si-I concentration was found to be 6 at atmospheric pressure [3, 21, n1,n2]. This ratio decreases as it was theoretically proved in this paper and experimentally found by other researchers [3].

Conclusion:

Very little scientific work has been done on pulse shaping or double pulse laser ablation effects on nanoparticles aggregates using MHz repetition rates. Using this effect to change the physical properties of pulses and to increase yield is also a very important advantage. We explored the effects of pulse energy and the ratio of Si⁺/Si that make up the aggregates. Our theoretical results closely predicted the general distribution of the Si-I and Si-II (Si,Si⁺) nanoparticles observed experimentally. We have also looked at the effects of pulse energy ratios on the size of nanoparticles and demonstrated experimentally that they agree with the fundamentals of interaction between femtosecond lasers and materials such as Silicon.

Should be written in MSword.

NOMENCLATURE

C	heat capacity per unit volume, $\text{J}/\text{m}^3 \text{ K}$	t_{Eq}^*	dimensionless equilibration time ($= t_{\text{Eq}}/t_P$)
E_g	band gap, eV	t_P	pulse duration time, s
h	Planck constant ($= 6.6262 \times 10^{-34}$), J s	T_C, T_L	temperature of carrier and lattice, respectively, K
I	laser intensity, W/m^2	α	absorption coefficient, m^{-1}
J	laser fluence, mJ/cm^2	α_1	one photon band-to-band absorption coefficient, m^{-1}
k_B	Boltzmann constant ($= 1.38066 \times 10^{-23}$), J/K	γ	Auger recombination coefficient, $\text{m}^6 \text{ s}^{-1}$
L	thickness of a silicon film, m	κ	thermal conductivity, $\text{W}/\text{m K}$
N_C	carrier number density, m^{-3}	λ	wavelength, m
R	reflectivity	ν	photon frequency, s^{-1}
t	time, s	τ_C	energy relaxation time, s
t_{Eq}	equilibration time, s		

REFERENCES (*Not the complete list- there are about 8-12 more*)

V. Narayanan, R.K. Thareja, Applied Surface Science 222 (2004) 382–393

Claeysens, Henley, and Ashfold, J. Appl. Phys., Vol. 94, No. 4, 15 August 2003

[] Seong Hyuk Lee et al, Numerical Heat Transfer, Part A, 44: 833–850, (2003)

[25] J.J. Chang, B.E. Warner, Appl. Phys. Lett. 69 (1996) 473.

[15] H. M. van Driel, Kinetics of High-Density Plasmas Generated in Si by 1.06- and 0.53-mm Picosecond Laser Pulses, Phys. Rev. B, vol. 35, pp. 8166–8176, (1987)

[19] D. Agassi, Phenomenological Model for Picosecond Pulse Laser Annealing of Semiconductors, J. Appl. Phys., vol. 55, pp. 4376–4383, (1984)

[21] J. R. Meyer, M. R. Kruer, and F. J. Bartoli, Optical Heating in Semiconductors: Laser Damage in Ge, Si, InSb and GaAs, J. Appl. Phys., vol. 51, pp. 5513–5522, (1980)

[] Ihtesham H. Chowdhury and Xianfan Xu sity,
“Figure (4) - Plot of surface lattice temperature as a function of time for a 100-fs FWHM pulse at four different fluence levels.” Numerical Heat Transfer, Copyright - Taylor & Francis Inc. Part A, 44: 219–232, (2003)

[32] J.R. Ho, C.P. Grigoropoulos, J.A.C. Humphrey, J. Appl. Phys.79 (1996) 156.

[33] A.V. Kabashin, M. Neunier, Appl. Phys. Lett. 82 (2003) 1619.

Will be deleted from this point onwards.

Proof of Si⁺/Si ratio by other researchers (incomplete list). The maximum production of nanoparticles occur, when the target is supplied with an Energy Ratio of 4-6 for the primary and the secondary pulses.

From : V. Narayanan, R.K. Thareja / *Applied Surface Science* 222 (2004) 382–393

(Not part of paper from here onward) - This information is substantiated by the previous researchers

Optical emission spectroscopy (OES) of the ablated silicon showed the presence of mostly Si I and Si II. The relative concentration of Si II/Si I decrease away from the target surface. The optimization of neutral concentration found at large distances from the target may be helpful in the formation of nanocrystalline silicon.

we observed Si I transitions as far as 22 mm from the target surface with the relative concentration of **Si II/Si I being 70 at 2 mm in 1 Torr of helium compared to 6 in atmospheric pressure.** The Si I species was observed at late times compared to Si II species. The observed spectrum in Fig. [] shows the formation of Si I after 50 ns and lasting till 450 ns whereas Si II has maximum intensity at 50 ns which disappears after 150 ns implying that Si I originates from recombination of Si II. This suggest that the nucleation of cluster starts with Si I, which, after condensation, gets deposited onto the suitably placed substrate. **Si II/Si I = 6 (but decreases with time since Si-II population decreases after 50 ns**

--

<i>Phys. Chem. Chem. Phys.</i> , 2005, 7, 3811–3818	3817
---	------

Variation of particle size due to laser repetition rate;

- The first point is 50 nm (calculated from the width of the aggregate wires and measured)
- The first point has 8 clusters

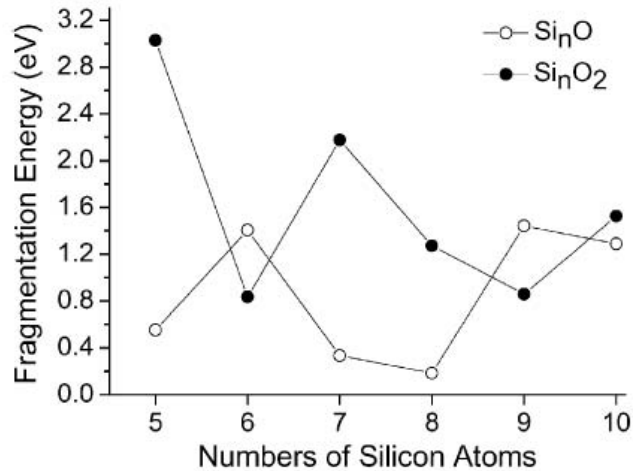


Fig. 6 Dissociation energies, defined by $DE = E(\text{Si}_k\text{O}_l) + E(\text{Si}_{n-k}\text{O}_{m-1}) - E(\text{Si}_n\text{O}_m)$, for the most favorable fragmentation channels of Si_nO and Si_nO_2 clusters.

1.2 / 0.2 (for **8** Si Atoms) = **6** (*Minimum allowed atoms according to Asiminov et al.*)

2.2 / 0.3 (for **7** Si Atoms) = **7.3**

1.4 / 0.8 (for **9** Si Atoms) = **1.75**

2.9 / 0.6 (for **5** Si Atoms) = **4.8**

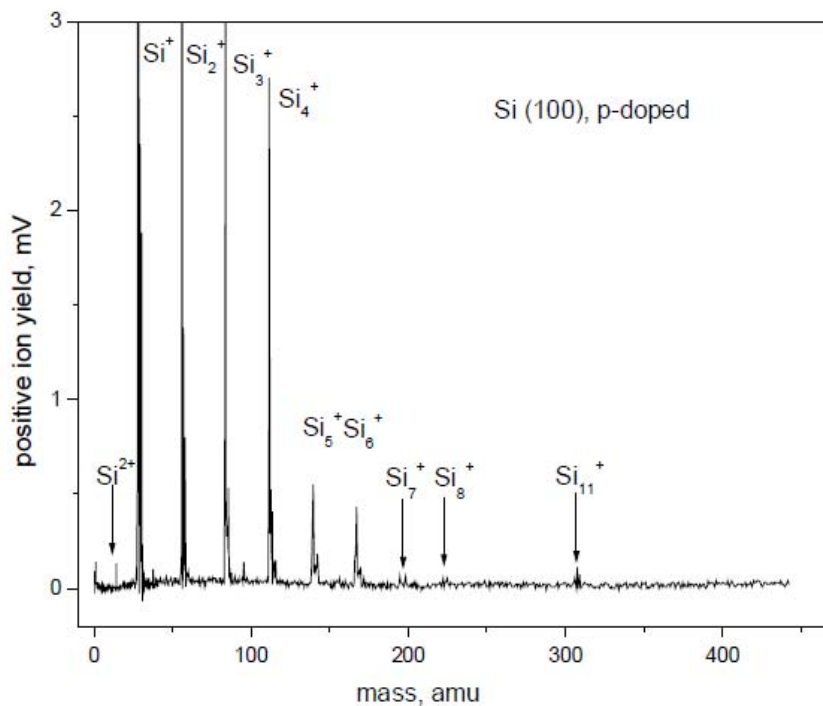


Fig. 1. T-o-F spectrum of positive ions emitted from p-Si (001) upon femtosecond ablation at $0.4 \times 10^{12} \text{ W/cm}^2$. Singly charged clusters up to $(\text{Si}_{11})^+$ as well as atomic Si^{2+} are observed. Note that, in fact, Si^+ is by far the most abundant ion (cut-off signals: Si^+ : 25 mV, Si_2^+ : 6 mV, Si_3^+ : 5 mV). (For this spectrum, we further improved the resolution and sensitivity by an electrostatic lens)

REFERENCES

V. Narayanan, R.K. Thareja, *Applied Surface Science* 222 (2004) 382–393

Claeysens, Henley, and Ashfold, *J. Appl. Phys.*, Vol. 94, No. 4, 15 August 2003

[] Seong Hyuk Lee et al, *Numerical Heat Transfer, Part A*, 44: 833–850, (2003)

[25] J.J. Chang, B.E. Warner, Appl. Phys. Lett. 69 (1996) 473.

[15] H. M. van Driel, Kinetics of High-Density Plasmas Generated in Si by 1.06- and 0.53-mm Picosecond Laser Pulses, Phys. Rev. B, vol. 35, pp. 8166–8176, (1987)

[19] D. Agassi, Phenomenological Model for Picosecond Pulse Laser Annealing of Semiconductors, J. Appl. Phys., vol. 55, pp. 4376–4383, (1984)

[21] J. R. Meyer, M. R. Kruer, and F. J. Bartoli, Optical Heating in Semiconductors: Laser Damage in Ge, Si, InSb and GaAs, J. Appl. Phys., vol. 51, pp. 5513–5522, (1980)

[] Ihtesham H. Chowdhury and Xianfan Xu sity,
“Plot of surface lattice temperature as a function of time for a 100-fs FWHM pulse at four different fluence levels.”
Numerical Heat Transfer, Copyright - Taylor & Francis Inc. Part A, 44: 219–232, (2003)
